Journal of Non-Crystalline Solids 405 (2014) 188–195

Contents lists available at ScienceDirect

Journal of Non-Crystalline Solids

journal homepage: www.elsevier.com/ locate/ jnoncrysol

X-ray diffraction study of NaF nano-crystals in photo-thermo-refractive glass

Julien Lumeau [a,b,*], Karima Chamma [b], Larissa Glebova [b], Leonid B. Glebov [b]

[a] Aix Marseille Université, CNRS, Centrale Marseille, Institut Fresnel UMR 7249, 13013 Marseille, France
[b] CREOL, The College of Optics and Photonics, University of Central Florida, P.O. Box 162700, Orlando, FL 32816-2700, USA

ARTICLE INFO

Article history:
Received 23 July 2014
Received in revised form 10 September 2014
Accepted 15 September 2014
Available online xxxx

Keywords:
Crystallization;
XRD;
Optical glass;
Photosensitivity;
Scattering

ABSTRACT

PTR glass is a photosensitive silicate glass which imparts refractive index change after UV-exposure and thermal development. The origin of photosensitivity is explained by the precipitation of NaF crystals inside the glass matrix. While nucleation of NaF in PTR glass has been thoroughly studied, the mechanisms of growth of NaF crystals have drawn a limited interest. To study the NaF growth, several techniques were combined: optical spectroscopy, interferometry, DSC and XRD. It was found that the size of NaF crystals in UV-exposed PTR glass, as determined by the broadening of the diffraction lines does not exceed ~20 nm. The NaF crystals' growth is limited by the exhaustion of Na^+F^- within the glass matrix as well as the increase of the viscosity of the glass surrounding the crystals that act as a kinetics barrier for further growth. X-ray diffraction analysis of NaF powder allowed calculating the crystals' volume fraction and their average size. A combination of these parameters with Rayleigh scattering model allowed the prediction of scattering at any wavelength and any thermal treatment, proving that scattering is determined by single crystals.

1. Introduction

Photo-thermo-refractive (PTR) glass is a photosensitive Na–Al–Zn–K–F–Br-silicate glass, doped with Ce, Ag, Sb, and Sn, that undergoes a permanent refractive index change after UV-exposure followed by thermal treatment [1,2]. PTR glass has been used for the fabrication of various types of volume diffractive optical elements [3], and it finds a wide range of applications such as spectral beam combining, selection of transverse and longitudinal modes in laser resonators, beam deflectors, splitters and attenuators [4]. A tentative description of the photo-induced reactions can be summarized as [5]: (i) oxidation of Ce^{3+} and formation of metallic silver during exposure to UV-radiation ($Ag^+ + Ce^{3+} \rightarrow Ag^0 + Ce^{4+}$), (ii) silver clustering during the first high temperature thermal treatment, and (iii) heterogeneous nucleation and growth of NaF nano-crystals on further heating. Other intermediate phases, such as AgBr or NaBr, for instance, might also form and thus the detailed nucleation mechanism of PTR glass is not yet clear [6]. Moreover, these substances are very hard to detect using conventional characterization techniques and might contribute to losses in PTR glass. In any case, after thermal treatment, PTR glass crystallizes partially, and a small fraction of nanometric NaF crystals appears embedded in the glass matrix [7,8]. This photo-thermo-induced crystallization in UV-exposed part is critical because NaF crystals are the cause for refractive index change [1–3]. However there are some associated drawbacks as these nano-crystals contribute to scattering losses within volume holographic elements (typically a few 0.1 to a few 1%).

Knowledge about the crystallization mechanisms involved in the photo-induced reactions in PTR glass throughout the various steps of thermal development is incomplete; a characterization of the complex crystallization process in such partially crystallized glass could shed some light into this matter. It should be noted that a thorough microstructural analysis of PTR glass is complicated due to the nano-metric scale (crystals typically are 20 nm in diameter) and small volume fraction (typically between 0.1 and 2 vol.%) of the phases formed after the standard low temperature thermal treatment processing used for the development of holographic optical elements. An important peculiarity of PTR glass is that nucleation and crystallization of NaF are controlled by the very low content of some key elements involved in the crystallization process, such as Ag, F and Br [9]. This fact must significantly impact the kinetics of phase formation, and hence is of great interest for a detailed study.

The aim of this study was to quantify the evolution of NaF crystals' parameters and correlate them with the optical characteristics of PTR glasses. In order to accomplish this, X-ray diffraction (XRD) technique was used for the evolution study of the crystal diameter, stress and volume fraction during the isothermal heat-treatment coupled with spectro-photometric measurement of scattering and interferometric measurement of refractive index change. Based on these results, the effect of NaF crystals on the refractive index change and scattering is assessed.

* Corresponding author at: Aix Marseille Université, CNRS, Centrale Marseille, Institut Fresnel UMR 7249, 13013 Marseille, France.
E-mail address: julien.lumeau@fresnel.fr (J. Lumeau).

http://dx.doi.org/10.1016/j.jnoncrysol.2014.09.019
0022-3093/

2. Experimental

2.1. PTR glass preparation

Samples of a photosensitive PTR glass containing $15Na_2O$–$5ZnO$–$4Al_2O_3$–$70SiO_2$–$5NaF$–$1KBr$–$0.01Ag_2O$–$0.01CeO_2$ (mol.%) and minor amounts of Sn and Sb were used in this work as in previous studies [7,10,11]. The glass was melted in an electric furnace in a 0.5 l platinum crucible at 1460 °C for 5 h in air and stirred using a Pt blade to homogenize the liquid. After melting, homogenizing and fining, the glass was cooled to the glass transition temperature (T_g ~ 460 °C), then annealed at T_g for 2 h, and cooled to room temperature at a rate of 0.1 K/min. Polished $25 \times 25 \times 2$ mm^3 samples were prepared from the batch. The chemical homogeneity of the samples is a critical parameter affecting crystallization properties [12], thus homogeneity was tested by the shadow method in a divergent beam of a He–Ne laser and was quantified by measurements using an interferometer (GPI Zygo). The samples selected for this study had refractive index fluctuations of less than 40 ppm (peak-to-valley) across the aperture.

2.2. UV-exposure and heat-treatments

UV-exposure of samples was performed by a He–Cd laser (4 mW, 325 nm). Each sample was exposed with maximum dosage of 0.9 J/cm^2 to a stripe with a single horizontal line scan and to a homogeneous squared area by scanning several overlapped lines on the sample [13]. The samples were first all nucleated for 100 min at 485 °C and then thermally developed at 515 °C for different time lengths varying from 1 to 72 h. All heat-treatments had the following sequence: temperature was elevated from room temperature to 485/515 °C at a rate of about 20 K/min where they were kept for the designed duration and then cooled down to room temperature in the furnace following the natural decrease of the furnace temperature (about 2.5 K/min). Finally, in order to remove any incipient crystallization on surfaces, each sample was ground and re-polished with flatness better than λ/2 at 633 nm.

2.3. Refractive index change measurements

Refractive index changes were measured in each sample using a shearing interferometer setup [13]. Its basic principle is to create an interferogram that converts the phase change at propagation through the glass to a fringe shift. A liquid cell with an index matching fluid was used to prevent thickness variations of the sample which would contribute to fringe shift. Therefore the interferometer fringe distortions resulted only from refractive index variations.

2.4. Spectra measurements

Transmission spectra were measured using a Perkin Elmer Lambda 950 spectro-photometer in the range from 200 to 1700 nm. Then, the spectral dependence of the losses coefficient was calculated by subtracting from the transmission spectra, the reflection spectrum of PTR glass that was calculated from the measured refractive index dispersion curve [14]. With the absolute precision of such spectro-photometric measurement being limited to about 2.10^{-2} cm^{-1} i.e. about one order of magnitude larger than its relative precision, each curve was calibrated. To achieve such, precise measurement of the transmission and the reflection at 1085 nm was carried out on each sample by photometric measurement using an Yb fiber laser. Then, losses were calculated at this wavelength, with a precision of 10^{-3} cm^{-1}, and all spectra were stitched to the measured value of losses at 1085 nm. Using this technique, the absolute precision of each spectrum was improved to 10^{-3} cm^{-1}. Also, as spectro-photometric measurements do not allow separating absorption losses from scattering losses, and the main source of absorption is associated with the presence of the plasmon resonance of Ag containing particles [15], all samples were bleached twice using a focused beam from the second harmonic from a Nd:YAG laser in order to remove the main part of the absorption [16]. That way, it can be shown that more than 90% of the losses measured above 400 nm are only associated with scattering losses. Finally scattering at 633 nm was extracted by fitting each curve with an exponential function as it was shown that this model allows accurate description of the spectral dependence of scattering in PTR glass [15]:

$$S(\lambda) = S_0 \left[\frac{\lambda_0}{\lambda}\right]^4 \text{ with } \lambda_0 = 633 \text{ nm}. \quad (1)$$

2.5. X-ray diffraction measurements

X-ray powder diffraction measurements were performed at room temperature on a Rigaku MiniFlex II using CuKα radiation (λ = 0.15418 nm), with a tube voltage of 30 kV and a tube current of 15 mA. The irradiated and bleached glass samples were pounded to a powder then sieved and the 45 to 75 μm size fraction was packed in a 2 mm deep indented quartz holder. Powdered samples were used in order to obtain samples with similar properties and avoid problems with NaF depleted layer close to the surface [12] that induce larger dispersion in the results than powdered samples. X-ray diffraction patterns were recorded for a 2Θ scan angle between 20 and 75° in a continuous scan mode with 0.02° sampling width and 0.2 deg/min scan rate. Corrections were made for instrument broadening. Each diffraction pattern showed similar features:

- An amorphous peak 2Θ from α-quartz at 22.80°
- Three crystalline diffraction peaks 2Θ, identified as sodium fluoride villiaumite
  - (200) at 38.55°
  - (220) at 55.65°
  - (222) at 69.85°.

The (200) peak around 38.55° is the main diffraction peak. To collect more detailed data, a second XRD run was performed at a lower scan rate of 0.02 deg/min from 37.5 to 39.5° 2Θ, and all subsequent analyses were carried out on this last measurement.

3. Results

3.1. Evolution of refractive index change and scattering in the process of thermal treatment

Table 1 shows the evolution of the refractive index change (RIC) as a function of the thermal treatment duration. Refractive index change values start reaching saturation at around 1000 ppm for 6 hour thermal treatment time. One must remember that refractive index change is defined as the difference of refractive index between UV-exposed and unexposed parts of a PTR glass. For thermal treatment durations higher than 6 h the saturation is associated with the beginning of crystallization of the unexposed part (associated with homogeneous nucleation) which prevents from carrying out any measurement and makes the

Table 1
Evolution of the refractive index change versus thermal treatment duration at 515 °C in PTR glass exposed to 0.9 J/cm^2 at 325 nm and pre-nucleated for 100 min at 485 °C.

Thermal treatment duration, hours	RIC, ppm
1	329
1.5	546
2	649
3	809
4	873
5	905
6	957

Table 2
Evolution of the scattering losses at 663 nm versus thermal treatment duration at 515 °C in PTR glass exposed to 0.9 J/cm^2 at 325 nm and pre-nucleated for 100 min at 485 °C.

Thermal treatment duration, hours	Scattering @ 633 nm, cm^{-1}
1	0.079
1.5	0.115
2	0.154
3	0.211
4	0.248
5	0.319
6	0.331
12	0.411
24	0.513
32	0.467
72	0.412

glass unusable for any optical application. Table 2 shows the temporal evolution of scattering at 633 nm. It can be seen that scattering increases for the first 24 h close to saturation value, then tends to decrease for the longer thermal treatment time of 36 and 72 h.

3.2. Evolution and processing of the X-ray diffraction peaks of NaF crystals

Fig. 1 shows the evolution of the main diffraction peak of NaF at ~38.5°. One can observe several remarkable features: First each of the diffraction peak exhibits a complex pattern composed by at least two different diffracted bands. Overall the amplitude of each diffracted peak increases when increasing the heat-treatment duration. Visually, no significant change in the width can be simply observed while the overall peak tends to shift towards larger angles (faint effect). To refine this analysis, calculations were performed on each diffraction pattern. The observed peak shapes are best described by peak shape functions. The most commonly used peak shape functions are as follows: Gaussian functions [17], Lorentzian functions [17], or Pseudo–Voigt, i.e. a combination of both [17]. In our case the best and most convenient model is the simple Gaussian distribution:

$$I^G_{i,k} = G_0 \exp\left(-\frac{(2\theta_i - 2\theta_i)^2}{2\sigma_\theta{}^2}\right) \quad (2)$$

where σ_θ is the FWHM, $2\theta_i$ is the Bragg angle of #i point and $2\theta_k$ is the calculated Bragg angle. To fit each diffraction peak, the background was first subtracted. Since the CuKα radiation is not strictly monochromatic, the Bragg peak is a convolution of the individual $K_{\alpha1}$ and $K_{\alpha2}$ peaks with the respective wavelengths $\lambda_1 = 1.54406$ Å and $\lambda_2 = 1.5444$ Å, and therefore it was necessary to perform a $K_{\alpha2}$ stripping.

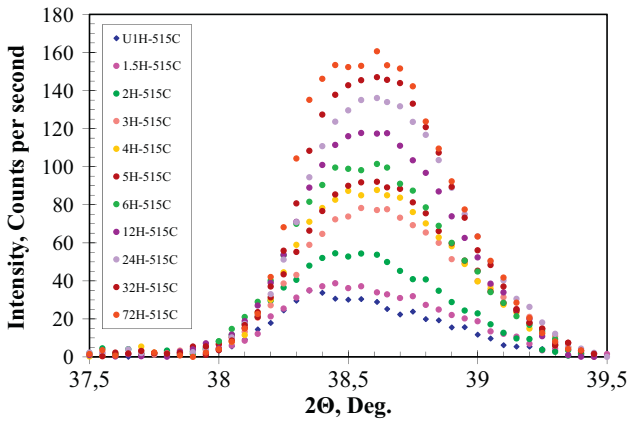

Fig. 1. Evolution of the X-ray diffraction peak of NaF crystals measured in PTR glass exposed to 0.9 J/cm^2 at 325 nm, pre-nucleated for 100 min at 485 °C and thermally developed at 515 °C for different durations.

Since every $K_{\alpha1}/K_{\alpha2}$ double peak is caused by scattering from a single lattice point, the *d*-spacing remains constant and the scattered intensity is proportional to the intensities of the two components. Using Bragg's law, the relationship between the positions of the diffracted peaks in the doublet is defined by: $\sin\Theta_1 / \lambda_{K\alpha1} = \sin\Theta_2 / \lambda_{K\alpha2}$. In addition, their integrated intensities are related as: $I^G(K\alpha_1) = 2I^G(K\alpha_2)$. Finally, common assumption that both peaks have identical shapes at lower diffraction angles was made [17]. Using the parameters of the Gaussian function used to fit the $K_{\alpha1}$ peak, the peak position, 2Θ, the peak position intensity, I, the crystallite diameter, D and the crystallite fraction volume fraction, V_f were estimated. Typical decomposition of the (200) diffraction peak of NaF powder is shown in Fig. 2-a and b, and Fig. 2-c shows similar fit performed on (200) peak measured after, respectively, 2 and 6 h at 515 °C. While this model could not take into account some of the fine features of the diffraction pattern, the overall shape could be well represented with such a simple model. From the fitted parameters for $K\alpha_1$, the evolution of the peak intensity, its position and the full width at half maximum during the crystallization process were, respectively, plotted in Fig. 3-a, b and c. Such an evolution is the signature of a change of the volume fraction, the crystal size and the stress surrounding each crystal during the thermal treatment process. The area under the diffraction peak was also calculated for all heat-treatment durations in both unexposed and UV-exposed glass. It is well known that this area is proportional to the volume fraction of crystals generated in the glass ceramics [17]. In order to extract the later parameter, a calibration curve was created by mixing virgin PTR glass powder with different known volume fractions of NaF crystals (Fig. 4). It is worth noting that due to similar densities of NaF and PTR glass, volume fractions of NaF in vol.% are only 10% higher than the fraction of NaF in wt.%. The evolution of the area under the curve as a function of the volume fraction of NaF crystals in wt.% can be accurately fitted using a linear function with a slope equal to 35.6 area-unit/wt.%. Using this calibration curve, the dependence of NaF crystals' volume fraction on thermal treatment duration was calculated and plotted in Fig. 5 for both unexposed and UV-exposed glass. The volume fraction evolution of UV-exposed PTR glass is similar to that of the peak intensity. Moreover, crystallization of unexposed PTR glass occurs after some longer induction time corresponding to the refractive index change saturation.

4. Discussion

The evolution of the optical and structural properties of PTR glass was presented. This section presents some further analysis of these data and a correlation between these optical and structural properties. First of all, from the position of the diffraction peak as shown in Fig. 3-b, the stress surrounding the NaF crystals could be extracted. It is known that radial stress surrounding the crystals produces a shift of the diffraction peak [18]. A shift towards lower angle corresponds to stretched crystals. Stress calculation can be performed using the following formulae:

$$\sigma = \frac{E_p}{\left(1-2\nu_p\right)}\frac{\Delta d}{d}. \quad (3)$$

Bragg law:

$$n\lambda = 2d\sin(\theta) \quad (4)$$

where E_p is the Young's modulus, ν_p is the Poisson ratio, $\Delta d/d$ is the relative change of the NaF lattice parameter, λ is the X-ray radiation wavelength and θ is the Bragg angle. Calculation shows that after 1 h of thermal treatment at 515 °C, stress is equal to ~1.3 GPa while after 72 h, stress is decreased to ~900 MPa. In other words, relaxation of the NaF crystals happens during the thermal treatment. It is important to note that the measured stresses are similar to the one measured by

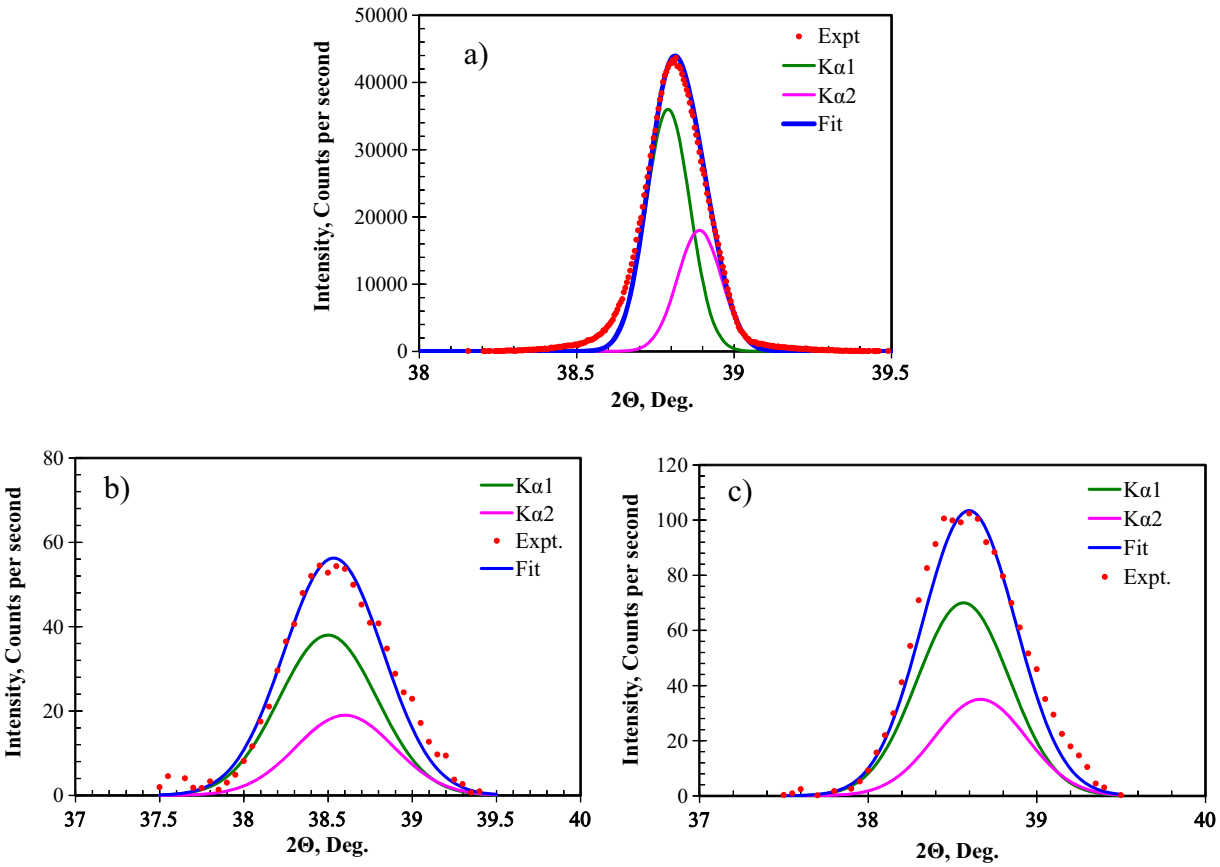

Fig. 2. Modeling of the X-ray diffraction peak of NaF crystals measured in a) pure NaF crystal powder b) PTR glass exposed to 0.9 J/cm^2 at 325 nm, pre-nucleated for 100 min at 485 °C and thermally developed for 2 h at 515 °C c) similar PTR glass as b) but thermally developed for 6 h at 515 °C.

NMR [19] or by synchrotron [18]. Moreover, this stress is a key parameter in the photo-thermo-refractivity of PTR glass as it was shown to play a major role in the appearance of refractive index change through the glass photo-elasticity [20].

Combining the data of Fig. 3-b and c allowed extracting one more parameter: the evolution of the mean crystal diameter using the Scherrer formula [21]:

$$D = K\lambda/(\sigma_1 \cos\theta) \tag{5}$$

$$\sigma_1^2 = \sigma_{\theta,1,\mathrm{exp}}^2 - \sigma_{\theta,1,\mathrm{inst}}^2 \tag{6}$$

where K is the Scherrer constant with a value of 1 for spherical particles, $\sigma_{\theta,1,\mathrm{exp}}$ is the FWHM measured on the sample, $\sigma_{\theta,1,\mathrm{inst}}$ is the instrument peak broadening that can be easily determined using crystalline NaF standard as shown in Fig. 2-a, θ is the Bragg angle and λ is the wavelength. Fig. 6 shows the evolution of the average crystal diameter as a function of thermal treatment duration. The average NaF crystal diameter increases until reaching saturation. However, one can see that the apparent diameter reaches 16 nm within the first hour then saturates to ~20 nm. This size limit is associated with the appearance of F-depleted zones surrounding each NaF crystals. Also, the growth of each individual crystals appears to occur very fast and to be a complex mechanism. The evolution of the volume fraction of crystals as a function of the thermal treatment duration was shown in Fig. 5. The volume fraction increases by 4 times when the heat treatment duration is increased from 1 to 72 h; this represents the saturation in crystal volume fraction that can be formed in this glass at this temperature [22], while the average crystal diameter only increases by 20% during the same thermal treatment period. Therefore, the increase of the crystals' volume fraction can only be explained by a combination of the increase of the crystals' average size and the increase of the crystal number density. Using basic chemistry equations and the NaF average crystal size, the evolution of the crystal number density and the evolution of the average distance separating the NaF crystals can be calculated. Using the expected concentration of NaF that is available for crystallization at this development temperature [22], it is possible to extract the NaF atomic concentration and the typical average distance between Na^+F^- atoms. Combining this parameter with the average NaF crystal diameter allows calculating, the average diameter of the Na^+F^--depleted glass zone, due to the creation and growth of NaF nano-crystals (Table 3). At saturation, the crystals have an average diameter of 20 nm and a density of 5×10^{21} m^{-3}. Saturation corresponds to a crystal-to-crystal distance comparable to the diameter of the NaF depleted zone of ~60 nm which corresponds to three times the crystal diameter. This average distance between crystals decreases during the thermal treatment and can very easily explain the data of the Fig. 3-b and calculated stresses surrounding NaF crystals. While this distance decreases, the interaction between the depleted zones increases, and this results in stress compensation of the glass and therefore affects the NaF crystals. It is also worth noting that the crystal number density reaches almost 50% of its value at saturation within the first hour of thermal treatment and that the average crystal diameter undergoes only a small change during the thermal treatment duration. This result shows that crystallization is a fast process at a 515 °C temperature. Glasses were nucleated for 100 min at 485 °C which allowed abundant nucleation of the glass and in turn triggered fast growth of 50% of the crystals within the first hour of the thermal treatment. But, due to the limited amount of fluorine in the glass, the NaF

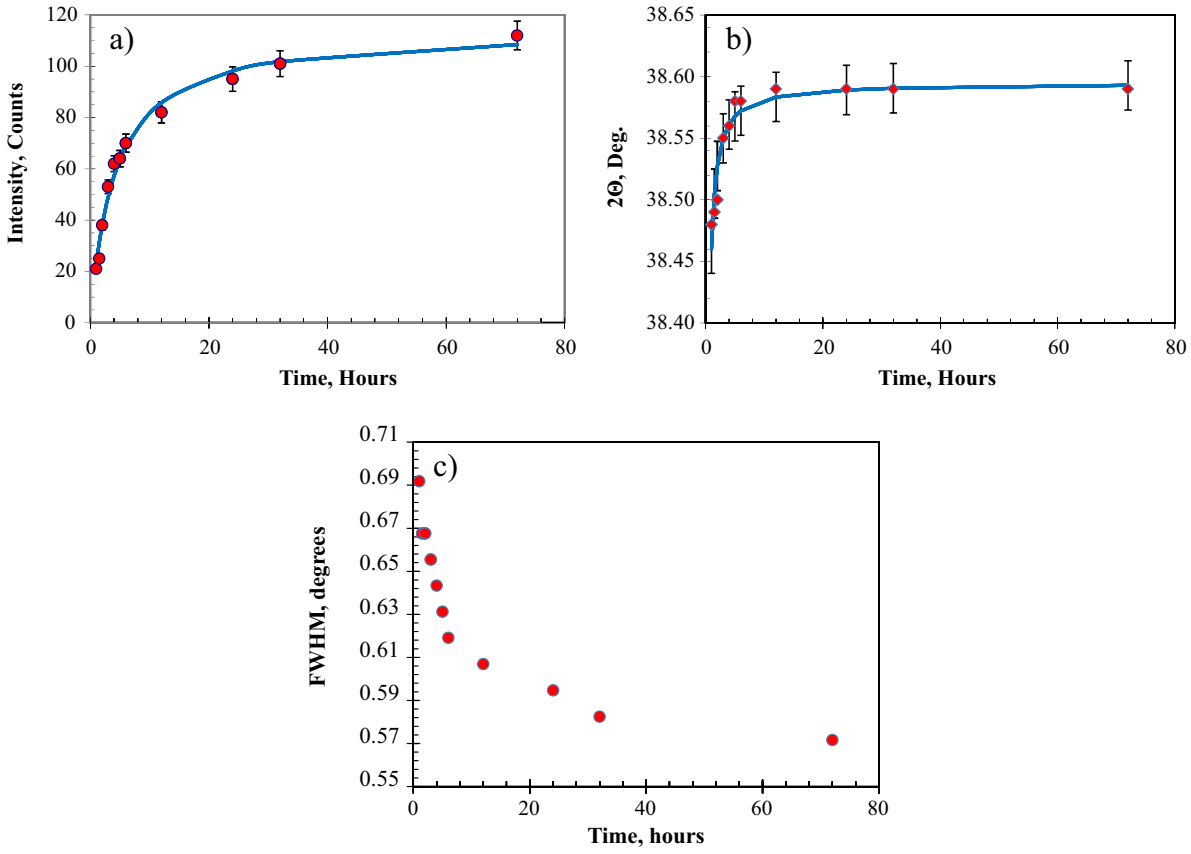

Fig. 3. Evolution of the parameters (peak intensity (a), position (b) and FWHM (c)) extracted from the X-ray diffraction peak of NaF crystals measured in PTR glass exposed to 0.9 J/cm^2 at 325 nm, pre-nucleated for 100 min at 485 °C and thermally developed at 515 °C for different durations (extracted from Kα_1).

exhaustion will impact both the nucleation rate (major effect) and the crystal growth rate. Therefore the mentioned crystals cannot grow at 515 °C to diameters much larger than 20 nm and the increase of the volume fraction of NaF crystals is therefore explained by further slow nucleation and growth of NaF nano-crystals on these new sites.

Using the data of Figs. 5 and 6 some additional calculations were performed. Table 2 presents the evolution of scattering as a function of thermal treatment duration. Scattering in PTR glass appears only after the glass has been exposed and developed at high temperature, and NaF nano-crystals, which have a refractive index (1.32) lower than the one of the glass matrix (1.5), have been created. It was shown in Ref. [15] that scattering is a spectral dependence following a λ^{-4} law typical of classical Rayleigh scattering [23]. Rayleigh scattering regime is defined by scattering from objects with a size which is much smaller than the wavelength of the light. In this case scattering has a linear dependence on the volume fraction of crystals and fourth power dependence on the crystal radius as follows:

$$S \propto V_f r^4 \tag{7}$$

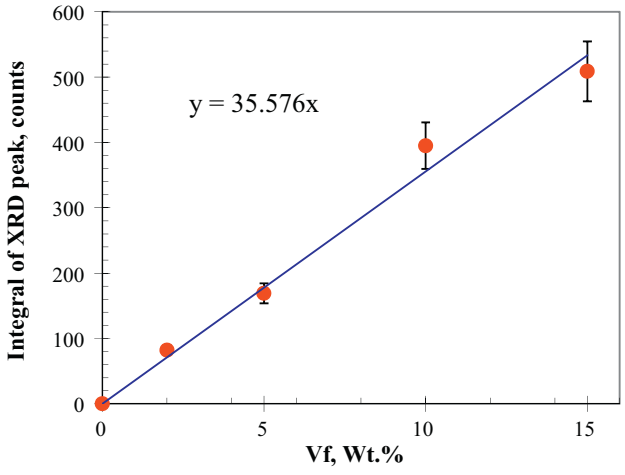

Fig. 4. Calibration curve for the volume fraction of NaF crystals measured by mixing virgin PTR glass powder with known volume fraction of pure NaF crystals powder and measuring the X-ray diffraction pattern.

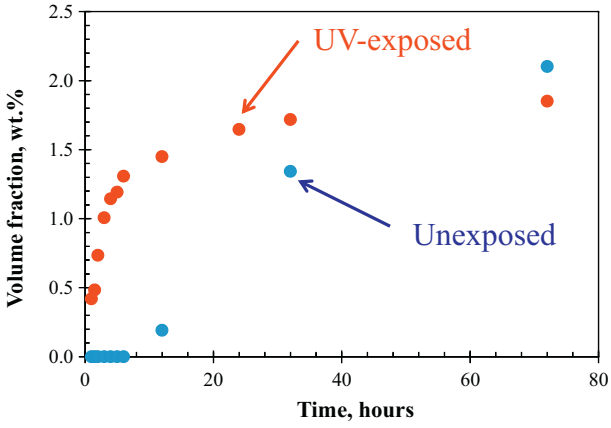

Fig. 5. Evolution of the volume fraction of NaF crystals measured in PTR glass exposed to 0.9 J/cm^2 at 325 nm, pre-nucleated for 100 min at 485 °C and thermally developed at 515 °C for different durations (red curve). For reference the evolution of the volume fraction of NaF crystals measured in unexposed PTR glass thermally treated in the same condition is shown (blue curve). (For interpretation of the references to color in this figure legend, the reader is referred to the web version of this article.)

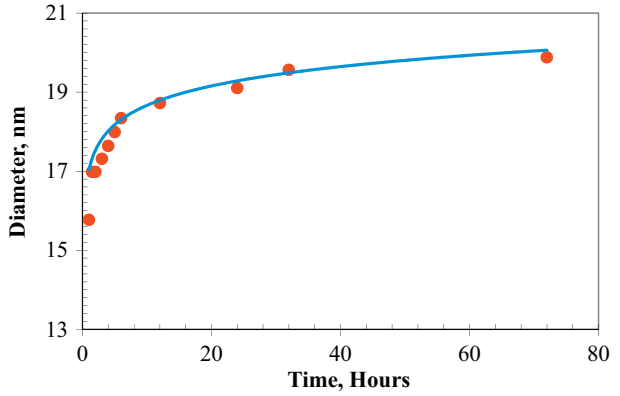

Fig. 6. Evolution of the average NaF crystal diameter extracted from the NaF X-ray diffraction peak measured in PTR glass exposed to 0.9 J/cm^2 at 325 nm, pre-nucleated for 100 min at 485 °C and thermally developed at 515 °C for different durations.

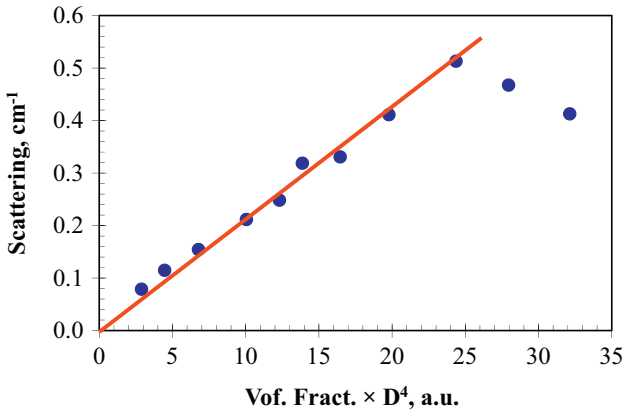

Fig. 7. Evolution of the scattering at 633 nm measured in PTR glass exposed to 0.9 J/cm^2 at 325 nm, pre-nucleated for 100 min at 485 °C and thermally developed at 515 °C for different durations (blue dots) as a function of the product between the NaF crystals volume fraction and the fourth power of the crystal radius, and its fit using a linear function (red line). (For interpretation of the references to color in this figure legend, the reader is referred to the web version of this article.)

where V_f is the volume fraction of crystals and r is the average NaF radius. In order to confirm that scattering is produced by individual NaF crystals and not by clusters of crystals or any other sites with a refractive index different from that of the glass matrix (such as droplets produced by liquid–liquid phase separation [24]), the dependence of scattering on $V_f r^4$ was plotted in Fig. 7. Except for the last two experimental points, the scattering losses have a linear dependence on $V_f r^4$, confirming that scattering is produced by individual NaF crystals. Further analysis have also shown that based on the volume fraction of crystals, their size and the refractive index contrast between NaF crystals and glass matrix, it is possible to fully model (using the radiation transfer theory) and predict scattering losses for any thermal treatment with duration less than 24 h. The loss of linear dependence of scattering on $V_f r^4$ for thermal treatment with a duration of more than 24 h can then be attributed to two effects: first, liquid–liquid phase separation is very likely to occur and to contribute to a different type of scattering that cannot be predicted by Rayleigh scattering [24]; moreover, when the glass is close to be depleted in Na^+F^-, the growth rate decreases resulting in a shift to a coarsening (or Ostwald ripening) regime [25]. This new regime results in the creation of dendrites which cannot be easily characterized by X-ray diffraction and cannot be modeled using Rayleigh scattering model. The relation between the refractive index change and the volume fraction of crystals and size was also investigated. It was shown in Ref. [7] that refractive index linearly depends on volume fraction of NaF crystals. To confirm this data, the dependence of refractive index change on NaF crystals' volume fraction was plotted in Fig. 8. In a first approximation, the refractive index change is in part linearly dependent on NaF crystals' volume fraction. However, there are some deviations from linearity that can be related to the mechanisms of refractive index change in PTR glass. Actually, as already mentioned above, refractive index changes in homogeneously exposed glasses are mostly due to stresses surrounding NaF nano-crystals [20]. In addition, from Fig. 3-b, it was shown that stress is not constant during the thermal treatment duration. Therefore, refractive index change can only partially be a function of the crystal volume fraction.

The cause of the NaF crystals' size saturation at ~20 nm was finally investigated. PTR glass samples were exposed at 325 nm with a dosage of 0.9 J/cm^2, then iso-thermally heat-treated in a Differential Scanning Calorimeter (DSC) at different temperatures ranging from 515 to 600 °C and stopping the heat-treatment after overall crystallization occurred, i.e. a temperature distinctly above that of the end of the crystallization peak. Observation of these DSC treated samples (Fig. 9) shows that depending on the thermal treatment temperature, UV-exposed samples have dramatically different appearance; the samples heat-treated at temperatures of 570 °C or below are translucent, while the samples heat-treated at temperatures of 590 °C and above are opaque and whitish. This difference of appearance is associated with significantly different levels of scattering, showing that the size of the created

Table 3
Evolution of the volume fraction, crystal diameter, crystal number density, average distance between crystals and the diameter of the depleted zones as a function of thermal treatment duration at 515 °C in PTR glass UV-exposed with 0.9 J/cm^2. It should be noted that the volume fraction of crystals at 72 h gives the reasonable agreement with data on NaF solubility in Ref. [22].

		D-NaF atoms	0.95	nm	
		a-NaF	0.33	nm	
Thermal treatment duration, hours	Volume fraction, vol.%	Crystal diameter, nm	Number of crystals per m^3	Distance between NaF crystals, nm	Diameter depleted zones, nm
1	0.47	15.77	2.27×10^{21}	76.05	45.60
1.5	0.54	16.98	2.10×10^{21}	78.14	49.10
2	0.82	16.98	3.19×10^{21}	67.95	49.10
3	1.12	17.31	4.12×10^{21}	62.36	50.05
4	1.27	17.64	4.43×10^{21}	60.91	51.01
5	1.33	17.99	4.35×10^{21}	61.27	52.02
6	1.45	18.34	4.50×10^{21}	60.55	53.03
12	1.61	18.72	4.69×10^{21}	59.74	54.13
24	1.83	19.1	5.02×10^{21}	58.40	55.23
32	1.91	19.56	4.87×10^{21}	58.98	56.56
72	2.06	19.88	5.00×10^{21}	58.47	57.48

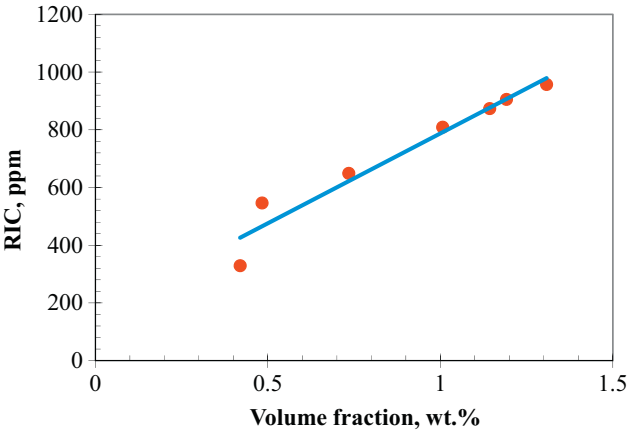

Fig. 8. Evolution of the refractive index change measured in PTR glass exposed to 0.9 J/cm^2 at 325 nm, pre-nucleated for 100 min at 485 °C and thermally developed at 515 °C for different durations as a function of the NaF crystals' volume fraction.

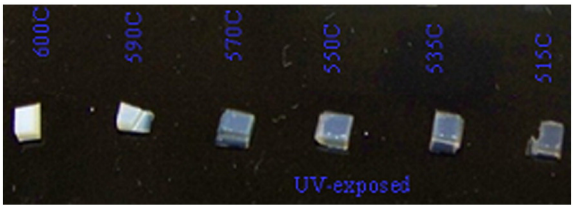

Fig. 9. Pictures of PTR glass samples exposed to 0.9 J/cm^2 at 325 nm, pre-nucleated for 100 min at 485 °C and isothermally treated in DSC at different temperature until reaching overall crystallization.

crystals is most probably different. To confirm this hypothesis, the X-ray diffraction patterns of samples heat-treated at 550 and 600 °C were measured and all the basic crystal parameters were extracted from these measurements (Table 4). First of all, the parameters measured in the sample heat-treated at 550 °C are very similar to the one measured in the sample heat-treated for 72 h at 515 °C that was studied previously, confirming that overall crystallization was achieved. However, the sample heat-treated at 600 °C shows different features; the volume fraction of crystals measured is comparable to that of the 550 °C heat-treated sample. The NaF solubility is comparable at 550 and 600 °C. Therefore, in both cases, overall crystallization was reached. However, after heat-treatment at 600 °C, the average crystal diameter is 30 nm, i.e. 50% larger than after 550 °C-heat-treatment (this size is probably limited by the peak broadening due to the apparatus function) and peak position is at a larger angle, which corresponds to a decrease of the stress surrounding these crystals (and these results correlate the results of Figs. 3-b and 6, i.e. the stress decreases while the average crystal diameter increases). Similar effect of limited growth was already observed in glasses with similar composition as PTR but with CaF_2 or BaF_2 nano-sized crystals and was explained by the presence of F-depleted diffusion-barrier zones surrounding each crystal. To analyze the results in PTR glass [26,27], one must take into account the structure presented in Ref. [20]. After thermal development, the glass has three different regions:

- The first area is a cubic sodium fluoride.
- As sodium and fluorine ions are consumed by the growing crystals, halos with the same components as virgin PTR glass, but are depleted in sodium and almost exhausted in fluorine, are formed.
- The third area, far away from the crystals, is an unperturbed glass region having identical composition as virgin PTR glass. The volume of this glass decreases as thermal treatment duration increases and is expected to have disappeared when all NaF has been consumed.

The region of interest is the intermediate region which has the composition of PTR glasses but is depleted in fluorine. Due to this depletion, the glass has an increased glass transition temperature with a value expected to be similar to the one of soda–lime silicate glasses, i.e. around 580 °C. This result could not be experimentally confirmed as decreasing the NaF content of PTR glass results in a fast increase of the temperature required for melting such a PTR glass which makes it hardly possible to melt with our technological capabilities. When glasses are developed below the glass transition temperature of this intermediate glass, it acts as a barrier for the growth of large NaF crystals, which explains the fast saturation of crystal diameter to a value of ~20 nm. When this glass transition temperature is overcome, further NaF crystal growth and coarsening can occur resulting in larger crystals and bulk scattering. Finally, it is important to remember that Souza et al. [7] demonstrated that dendritic growth occurs after high temperature heat-treatments. Such a growth induces large scattering as seen within this study, but it is also worth mentioning that in this case, the exact determination of the crystal size using Scherrer becomes inaccurate. This could maybe partially explain some disagreements in Fig. 7.

Table 4
Parameters measured by X-ray diffractometer in UV-exposed PTR glass developed at 550 °C and 600 °C after completing overall crystallization as measured by isothermal DSC.

Temperature, °C	2 theta, degree	FWHM, degree	Intensity, counts	Diameter, nm	Vf, wt.%
550	38.57	0.53	127	21	2
600	38.62	0.37	200	31	2.25

5. Conclusion

The NaF growth in PTR glass was studied by combining optical spectroscopy, interferometry, DSC and XRD. Those data were used in order to generate a simple model that allows correlating structural and optical data and could be used to predict the final performances of UV-exposed and thermally developed PTR glasses. The size of NaF crystals in UV-exposed PTR glass as determined by the broadening of diffraction lines was shown not to exceed ~20 nm. The NaF crystals' growth limiting parameter is the exhaustion of Na^+F^- within the glass matrix as well as the increase of the glass transition temperature of the glass surrounding the NaF crystals, and it acts as a barrier for further NaF crystal growth. Combining size and volume fraction of NaF crystals in PTR glass with Rayleigh scattering model allowed the prediction of scattering at any wavelength and thermal treatment schedule, proving that overall scattering is determined by the sum of the scattering of each individual crystals. Finally, due to the mechanisms at the origin of these changes, the dependence of the refractive index change on crystal volume fraction is only partially linear.

Acknowledgment

This work was supported by DARPA ADHELS (HR-0011-06-1-0010) project. We are thankful to Dr Dogariu's group for helping us in the analysis of the origin of scattering in PTR glasses.

References

[1] L.B. Glebov, N.V. Nikonorov, E.I. Panysheva, G.T. Petrovskii, V.V. Savvin, I.V. Tunimanova, V.A. Tsekhomskii, Polychromatic glasses — a new material for recording volume phase holograms, Sov. Phys. Dokl. 35 (1990) 878–880.
[2] L.B. Glebov, Photochromic and photo-thermo-refractive (PTR) glasses, Encyclopedia of Smart Materials, John Wiley & Sons, New York, 2002.
[3] O. M. Efimov, L. B. Glebov, V. I. Smirnov, High efficiency volume diffractive elements in photo-thermo-refractive glass, Patent No. US 6,673,497 B2. January 6, 2004.
[4] L.B. Glebov, V.I. Smirnov, C.M. Stickley, I.V. Ciapurin, New approach to robust optics for HEL systems in Laser Weapons Technology III, in: W.E. Tompson, P.H. Merritt (Eds.), Proceedings of SPIE, vol. 4724, 2002, pp. 101–109.
[5] S.D. Stookey, Photosensitive glass, a new photographic medium, Ind. Eng. Chem. 41 (1949) 856–861.
[6] I. Dyamant, A.S. Abyzov, V.M. Fokin, E.D. Zanotto, J. Lumeau, L.N. Glebova, L.B. Glebov, Crystal nucleation and growth kinetics of NaF in photo-thermo-refractive glass, J. Non-Cryst. Solids 378 (2013) 115–120.
[7] T. Cardinal, O.M. Efimov, H.G. Francois-Saint-Cyr, L.B. Glebov, L.N. Glebova, V.I. Smirnov, Comparative study of photo-induced variations of X-ray diffraction and refractive index in photo-thermo-refractive glass, J. Non-Cryst. Solids 235 (2003) 275–281.
[8] G.P. Souza, V.M. Fokin, E.D. Zanotto, J. Lumeau, L. Glebova, L.B. Glebov, Micro and nanostructures in partially crystallized photo-thermo-refractive glass, Phys. Chem. Glasses Eur. J. Glass Sci. Technol. B 50 (5) (2009) 311–320.
[9] L. Glebova, J. Lumeau, M. Klimov, E.D. Zanotto, L.B. Glebov, Role of bromine on the thermal and optical properties of photo-thermo-refractive glass, J. Non-Cryst. Solids 354 (2008) 456–461.
[10] O.M. Efimov, L.B. Glebov, S. Papernov, A.W. Schmid, Laser-induced damage in optical materials, Proc. SPIE, 3578, 1999, p. 554.
[11] O.M. Efimov, L.B. Glebov, V.I. Smirnov, Opt. Lett. 23 (2000) 1693.
[12] J. Lumeau, A. Sinitskii, L. Glebova, L.B. Glebov, E.D. Zanotto, Method to assess the homogeneity of partially crystallized glasses: application to a photo-thermo-refractive glass, J. Non-Cryst. Solids 355 (34–36) (2009) 1760–1768.
[13] Oleg M. Efimov, Leonid B. Glebov, Hervé P. Andre, Measurement of the induced refractive index in a photothermorefractive glass by a liquid-cell shearing interferometer, Appl. Opt. 41 (1864–1871) (2002).
[14] Refractive index dispersion in photo-thermo-refractive glass, CREOL Internal Report, 2009.
[15] J. Lumeau, L. Glebova, L. Glebov, Absorption and scattering in photo-thermo-refractive glass induced by UV exposure and thermal development, Opt. Mater. 36 (2014) 621–627.

[16] J. Lumeau, L.B. Glebov, Mechanisms of optical bleaching of silver containing particles in photo-thermo-refractive glass, Appl. Opt. (2014) (submitted for publication).
[17] Vitalij K. Pecharsky, Peter Y. Zavalij, Fundamentals of Powder Diffraction and Structural Characterization of Materials, Kluwer Academic Publishers, 2003.
[18] F.C. Serbena, G.P. Souza, E.D. Zanotto, J. Lumeau, L. Glebova, L.B. Glebov, Internal residual stress in partially crystallized photo-thermo-refractive glass, J. Am. Ceram. Soc. 94 (3) (2011) 671–674.
[19] J. Zwanziger, U. Werner-Zwanziger, E.D. Zanotto, E. Rotari, L.N. Glebova, L.B. Glebov, J.F. Schneider, J. Appl. Phys. 99 (2006) 083511.
[20] J. Lumeau, L. Glebova, L.B. Glebov, V. Golubkov, E.D. Zanotto, Origin of crystallization-induced refractive index changes in photo-thermo-refractive glass, Opt. Mater. 32 (2009) 139–146.
[21] A. Patterson, The Scherrer formula for X-ray particle size determination, Phys. Rev. 56 (10) (1939) 978–982.
[22] V.M. Fokin, G.P. Souza, E.D. Zanotto, J. Lumeau, L. Glebova, L.B. Glebov, Sodium fluoride solubility in photo-thermo-refractive glass, J. Am. Ceram. Soc. 93 (3) (2010) 716–721.
[23] C.F. Bohren, D. Huffman, Absorption and Scattering of Light by Small Particles, John Wiley, New York, 1983.
[24] G.P. Souza, V.M. Fokin, C.F. Rodrigues, A.C.M. Rodrigues, E.D. Zanotto, J. Lumeau, L. Glebova, L.B. Glebov, Liquid–liquid phase separation in photo-thermo-refractive glass, J. Am. Ceram. Soc. 94 (1) (2011) 145–150.
[25] Lorenz Ratke, Peter W. Voorhees, Growth and Coarsening: Ostwald Ripening in Material Processing, Springer, 2002.
[26] C. Rüssel, Nano-crystallization of CaF_2 from $Na_2O/K_2O/CaO/CaF_2/Al_2O_3/SiO_2$ glasses, Chem. Mater. 17 (2005) 5843–5847.
[27] C. Bocker, C. Rüssel, Self organized nano-crystallisation of BaF_2 from $Na_2O/K_2O/BaF_2/Al_2O_3/SiO_2$ glasses, J. Eur. Ceram. Soc. 29 (2009) 1221–1225.